

# THE INTERCALATION BEHAVIOUR AND PHYSICO-CHEMICAL CHARACTERISATION OF NOVEL INTERCALATED NANOCOMPOSITE FROM ZINC/ALUMINIUM LAYERED DOUBLE HYDROXIDES AND BROADLEAF HERBICIDE CLOPYRALID

Sharifah Norain Mohd Sharif<sup>1, 2, ✉</sup>, Illyas Md Isa<sup>1, 2</sup>,  
Mazidah Mamat<sup>3</sup>, Noorshida Mohd Ali<sup>1</sup>, Suriani Abu Bakar<sup>2, 4</sup>,  
Mohd Zobir Hussein<sup>5</sup>, Suzaliza Mustafar<sup>1</sup>

<https://doi.org/10.23939/chcht14.01.038>

**Abstract.** This study reports on the preparation of novel zinc/aluminium layered double hydroxide intercalated clopyralid (Zn/Al-LDH-CP) nanocomposites fabricated *via* co-precipitation. An expansion of the interlayer gallery of Zn/Al-LDH for the accommodation of clopyralid was observed from the powder X-ray diffraction (PXRD) pattern, confirming the occurrence of intercalation. The results from Fourier transform infrared and elemental analysis were consistent with those from PXRD, thus supporting the intercalation of clopyralid. The thermal studies showed that the nanocomposite had better thermal stability compared to pristine clopyralid. Based on these data, the chemical formula of the nanocomposite was proposed as  $[\text{Zn}_{0.75}\text{Al}_{0.25}(\text{OH})_2][\text{C}_5\text{H}_2\text{Cl}_2\text{NCOO}]_{0.25} \cdot 0.67\text{H}_2\text{O}$ , and the percentage loading of clopyralid in the interlayer gallery of Zn/Al-LDH was calculated to be 25.39%. These characterisation results indicate a very promising future for this novel Zn/Al-LDH-CP nanocomposite.

**Keywords:** zinc/aluminium layered double hydroxide, co-precipitation, clopyralid, intercalation, herbicide.

<sup>1</sup> Department of Chemistry, University Pendidikan Sultan Idris, 35900 Tanjong Malim, Perak, Malaysia

<sup>2</sup> Nanotechnology Research Centre, University Pendidikan Sultan Idris, 35900 Tanjong Malim, Perak, Malaysia

<sup>3</sup> Foundation of Science Study Centre, University Malaysia Terengganu,

21030 Kuala Terengganu, Terengganu, Malaysia

<sup>4</sup> Department of Physics, University Pendidikan Sultan Idris, 35900 Tanjong Malim, Perak, Malaysia

<sup>5</sup> Materials Synthesis and Characterization Laboratory, Institute of Advanced Technology, University Putra Malaysia, 43400 Serdang, Selangor, Malaysia

✉ [norhayati.hashim@fsm.upsi.edu.my](mailto:norhayati.hashim@fsm.upsi.edu.my)

© Sharif S., Hashim N., Isa I., Mamat M., Ali N., Bakar S., Hussein M., Mustafar S., 2020

## 1. Introduction

Nanocomposites are materials produced *via* hybridisation of different kinds of materials, and have at least one dimension on the nanometre scale [1]. Nanocomposites have been reported to exhibit qualities that distinguish them from their counterpart bulk materials, especially regarding thermal, mechanical, electronic, physico-chemical and functional properties, as well as sensitivity to surface processes, penetrability and reactivity [2-4]. One popular way to produce these nanocomposite materials is *via* intercalation [5-10].

Layered double hydroxides (LDH) are clay-like materials that have been widely used as host materials for the intercalation of various kind guest ions, as a method to synthesise nanocomposite materials. This is due to the large surface area, remarkable anion exchange capability, excellent biomedical properties, chemical inertness and low toxicity of LDH [3, 11]. LDH have the ability to intercalate guest anions into the interlayer gallery because they are composed of infinite sheets of positively charged brucite-type materials; but some of the divalent cations of the sheets have been substituted by tetrahedral cations in octahedral coordination. The general formula of LDH is  $[\text{M}^{2+}_{(1-x)}\text{L}^{3+}_x(\text{OH})_2]^{x+} \text{A}^{m-}_{x/m} \cdot n\text{H}_2\text{O}$ , where  $\text{M}^{2+}$  and  $\text{L}^{3+}$  represent divalent and trivalent metal cations, respectively, whereas  $\text{A}$  stands for the guest ion [12].

Several methods have been reported to intercalate guest ions into the interlayer gallery of LDH, such as ion exchange, co-precipitation and reconstruction methods [13-15]. Amongst these methods, co-precipitation seems to be the most frequently used in synthesising LDH, due to the fact that LDH can be directly intercalated with guest ions to produce well-crystallised nanocomposites [16-18]. This

method also allows for LDH-intercalated nanocomposite to be produced in huge quantities, by simply scaling up the starting material [19]. Due to the rapid growth in nanotechnology, the application of LDH-intercalated nanocomposites has been progressively developed in a wide range of applications, including adsorbents, catalysts, bactericides, sensors and controlled release formulations [20-29].

Clopyralid (CP), also known as 3,6-dichloro-2-pyridinecarboxylic acid, is a selective post-emergence weed control agent commonly used on sugar beets, field corn, small grains, fallow fields, pastures, rangeland, fir plantations, and non-crop plants [30, 31]. The chemical structure of clopyralid is shown in Fig. 1. Clopyralid is an auxin-mimic herbicide, as it mimics the plant growth hormone auxin, thus triggering uncontrolled and disorganised growth in the targeted weeds [32].

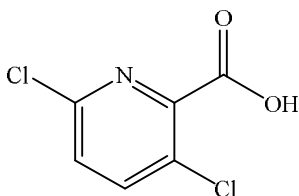


Fig. 1. Chemical structure of clopyralid

The present work examines the possibility of intercalating CP into the interlayer gallery of Zn/Al-LDH using the co-precipitation method. To the best of our knowledge, no study was yet reported on the successful intercalation of CP into this host layered material. Also, a characterisation study was performed on the novel nanocomposite Zn/Al-LDH-CP using several instruments, including powder X-ray diffraction (PXRD), Fourier transform infrared (FTIR), inductively coupled plasma optical emission spectrometry (ICP-OES), thermogravimetric analysis (TGA), gas sorption analysis, carbon, hydrogen, nitrogen and sulphur (CHNS) elemental analysis and field emission scanning electron microscopy (FESEM), so that the physico-chemical properties could be thoroughly investigated. The novel Zn/Al-LDH-CP nanocomposite is expected to benefit the agricultural sector in the future.

## 2. Experimental

### 2.1. Reagents

All reagents used in this work were purchased from various suppliers and used without further purification.  $Zn(NO_3)_2 \cdot 6H_2O$  (purity 98 %) and

$Al(NO_3)_3 \cdot 9H_2O$  (purity 98 %) were obtained from System. The herbicide CP was purchased from China (purity 95 %). The pH value of the solution was adjusted by the addition of NaOH and HCl, supplied by Merck and Sigma-Aldrich, respectively. Deionised water was used to prepare all aqueous solutions and the mixture was constantly bubbled with  $N_2$  gas throughout the preparation process to minimise contamination with atmospheric  $CO_2$ .

### 2.2. Synthesis of Zn/Al-LDH-CP Nanocomposite

The Zn/Al-LDH-CP nanocomposite was prepared using the co-precipitation method, in the presence of a constant flow of  $N_2$  gas [33]. A nitrate solution obtained by dissolution was prepared in 250 ml of deionised water from aqueous solutions of  $Zn(NO_3)_2 \cdot 6H_2O$  (0.1M) and  $Al(NO_3)_3 \cdot 9H_2O$  (0.033M) with the molar ratio  $R = 3$ . The pH value of the mixture was then adjusted to the desired pH ( $7.5 \pm 0.05$ ) and the mixture was vigorously stirred under a nitrogen atmosphere. Then, 100 ml of the CP solution (0.05, 0.1 or 0.2M) was simultaneously added to the mixture. A few drops of HCl were added to the mixture if necessary. The resulting suspension was aged at 343 K in an oil bath shaker for 24 h. The product was collected by centrifugation (40 rpm for 5 min), thoroughly rinsed with deionised water and dried in an oven at 333 K. Once the product was completely dried, the product was ground into a fine powder and denoted as the Zn/Al-LDH-CP nanocomposite.

### 2.3. Characterisation

The previously synthesised Zn/Al-LDH-CP nanocomposite was characterised by PXRD, FTIR, TGA, ICP-OES, CHNS elemental analysis, FESEM and gas sorption analysis. The PXRD patterns were obtained on a Bruker AXS model D8 Advance using  $Cu K_\alpha$  irradiation ( $\lambda = 0.15406$  nm) at 60 kV, 60 mA and  $0.025^\circ \cdot s^{-1}$  in the range of  $2-60^\circ$ . The FTIR spectra were recorded over the wavenumber range of  $400-4000$   $cm^{-1}$  on a Thermo Electron Corporation FTIR spectrophotometer. The samples were mixed with KBr and compressed into a thin disk before undergoing FTIR analysis. Further characterisation was provided by TGA, performed on a Perkin-Elmer Pyris 1 TGA Thermo Balance instrument where the samples were heated to 1273 K at a heating rate of  $10$   $K \cdot min^{-1}$  in a nitrogen atmosphere. For the quantification of the metallic elements zinc and aluminium, an ICP-OES model Perkin-Elmer Plasma 1000 was used, whereas the percentages of carbon, hydrogen and nitrogen were

determined using a CHNS elemental analyser, model CHNS-932 LECO. The morphology of the nanocomposite was studied by FESEM using a Hitachi SU 8020 UHR instrument. The surface properties of the samples were studied using a Quantachrome Autosorb automated gas sorption analyser by the nitrogen adsorption-desorption technique. The surface area was determined using the Brunauer-Emmett-Teller (BET) method, whereas the pore size distribution of each solid was determined using the classical Barret-Joyner-Halenda (BJH) method.

### 3. Results and Discussion

#### 3.1. PXRD Analysis

Fig. 2 shows the PXRD patterns of Zn/Al-LDH, CP, and its nanocomposite, Zn/Al-LDH-CP which were synthesised *via* the co-precipitation method at various concentrations of CP, ranging from 0.05 to 0.2 M. The PXRD pattern of Zn/Al-LDH revealed the typical characteristic of a Zn/Al-LDH (hydrotalcite-like) phase (JCPDS card No.51-1528). Three obvious peaks were observed in the PXRD pattern, with a basal spacing of 8.8, 4.4 and 2.8 Å, respectively. The presence of nitrate ions as the counterbalancing ions in the interlayer gallery of Zn/Al-LDH was recognised from the PXRD pattern, based on the existence of a peak with the basal spacing of 8.8 Å, which appeared at a low  $2\theta$  angle of  $9.8^\circ$  [34, 35]. The appearance of intense, sharp and symmetrical peaks indicated the crystalline structure of Zn/Al-LDH [36].

When CP was introduced into the mixture of  $\text{Zn}(\text{NO}_3)_2 \cdot 6\text{H}_2\text{O}$  and  $\text{Al}(\text{NO}_3)_3 \cdot 9\text{H}_2\text{O}$  during the co-precipitation reaction, the negatively charged carboxylate group in CP was attracted to the positively charged Zn/Al-LDH layer through an electrostatic attraction. The electrostatic attraction allowed CP to retain its position in the interlayer gallery of Zn/Al-LDH [37]. It was observed from the PXRD pattern that, after co-precipitation was performed, the basal spacing was expanded to 14.7–15.7 Å, thus indicating that CP was successfully intercalated into the interlayer gallery of Zn/Al-LDH. The enlargement of the basal spacing provided strong evidence of successful intercalation due to the fact that the interlayer distance is greatly dependent on the size of the incoming anion and the size of CP is significantly larger compared to nitrate ions [36]. The PXRD pattern of the Zn/Al-LDH-CP nanocomposite showed symmetrical, sharp and intense peaks, with basal spacing of 14.7–15.7, 7.7–7.8, 5.0–5.1 and 3.8 Å, which reveals that the nanocomposite was crystallised with a well-ordered layered structure.

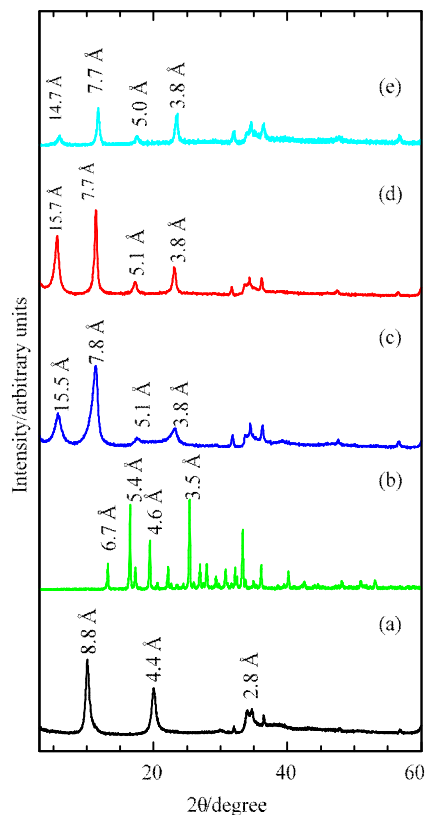


**Fig. 2.** PXRD patterns of Zn/Al-LDH (a), CP (b) and Zn/Al-LDH-CP nanocomposites prepared using 0.05 (c), 0.1 (d) and 0.2 (e) M CP

It was noticeable from the results obtained in the PXRD analysis that the synthesised Zn/Al-LDH-CP nanocomposites, the nanocomposite prepared using 0.1 M CP exhibited better intensity and crystallinity compared to the nanocomposites prepared using 0.05M and 0.2M. Therefore, this nanocomposite was selected for use in the characterisation study.

#### 3.2. Spatial Orientation of CP in Zn/Al-LDH Interlayer

Fig. 3 illustrates the three-dimensional molecular size of CP estimated using Chem 3D Ultra 8.0 software. The  $x$ ,  $y$  and  $z$  axis were calculated to be 8.5, 6.9 and 4.3 Å, respectively. Considering that the basal spacing obtained from the PXRD analysis (Fig. 2d) was 15.7 Å and the thickness of each Zn/Al-LDH layer was 4.8 Å, the height of the interlayer gallery after intercalation was determined to be 10.9 Å (Fig. 4) [38]. Hence, based on the three-dimensional size of CP and the height of the interlayer gallery, it can be proposed that the intercalated CP was oriented in the interlayer gallery of Zn/Al-LDH in a monolayer arrangement, maintained in their position via electrostatic interactions.

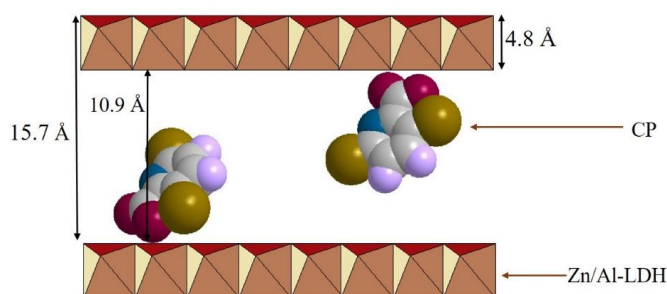


**Fig. 3.** Spatial orientation of CP in the interlayer gallery of Zn/Al-LDH

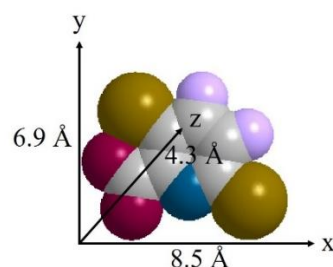


**Fig. 4.** Three-dimensional molecular structure of CP

### 3.3. FTIR Analysis

The infrared spectra of the samples are shown in Fig. 5. Zn/Al-LDH displayed a very strong peak at  $1385\text{ cm}^{-1}$  triggered by the vibration of the nitrate ion in the interlayer gallery of Zn/Al-LDH (Fig. 5a) [39]. The presence of a very broad peak centred at  $3450\text{ cm}^{-1}$  indicates that the hydroxyl group was found in both the interlayer water and the hydroxide basal layer [40]. Two weak peaks were also observed at  $604$  and  $432\text{ cm}^{-1}$ , resulting from the bending vibration of Al-OH and Zn-Al-OH, respectively [41].

The FTIR spectra show that there were several characteristic peaks of CP that could be clearly observed in the FTIR spectra of the Zn/Al-LDH-CP nanocomposite. The peaks attributed to C-N stretching mode in aromatic compounds were seen in the FTIR spectra of CP at  $1316\text{ cm}^{-1}$  and Zn/Al-LDH-CP at  $1333\text{ cm}^{-1}$ . A notable peak that denoted the stretching of C-O was also present in both FTIR of CP (at  $1146\text{ cm}^{-1}$ ) and the Zn/Al-LDH-CP nanocomposite (at  $1138\text{ cm}^{-1}$ ). The peaks at  $1561$  and  $1412\text{ cm}^{-1}$ , assigned to antisymmetric and symmetric stretching vibrations of the  $-\text{COO}-$  group in the pattern of CP, were found in the FTIR spectra of Zn/Al-LDH-CP at  $1401$  and  $1579\text{ cm}^{-1}$  [42]. The peak that signifies the stretching vibrations of carbonyl  $-\text{C}=\text{O}$  in  $-\text{COOH}$  group was observed in the FTIR spectra of pure CP at  $1718\text{ cm}^{-1}$ . We also observed a strong peak attributed to the presence of nitrate ions (peak at  $1385\text{ cm}^{-1}$  in Zn/Al-LDH) that was no longer found in the FTIR spectra of the Zn/Al-LDH-CP nanocomposite. The disappearance of the peak indicates that the CP anions had replaced the nitrate ions in the interlayer gallery [39]. This confirms the presence of CP in the Zn/Al-LDH-CP nanocomposite, though some peaks may have been slightly shifted due to the interaction between CP and Zn/Al-LDH as an intercalation took place [26].

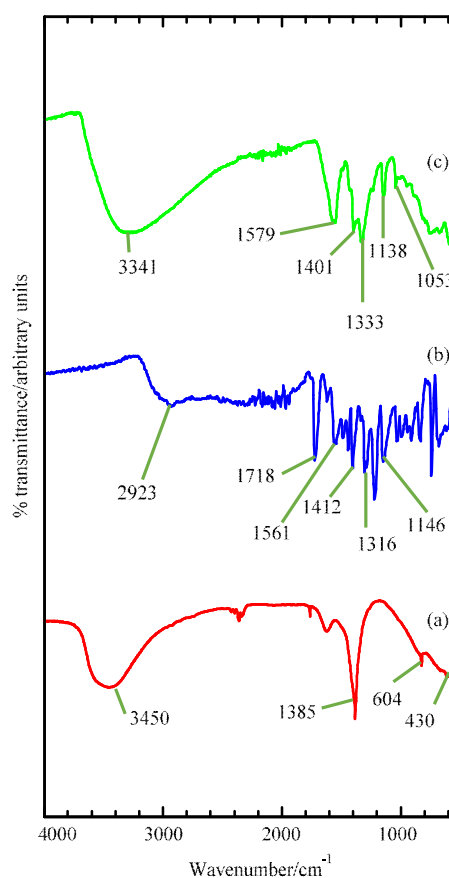


**Fig. 5.** FTIR spectra of Zn/Al-LDH (a), CP (b) and Zn/Al-LDH-CP (c) nanocomposites

### 3.4. Thermal Studies

During the thermal stability studies, the samples were heated from room temperature to  $1273\text{ K}$ . The rising temperature triggered the oxidation and decomposition of the samples, resulting in a weight loss. Then the reduction in the weight of the samples was analysed to indicate their thermal stability.

The results from the thermal stability studies on Zn/Al-LDH, pure CP and the Zn/Al-LDH-CP nanocomposite are illustrated in Fig. 6. Based on the TGA curve, the thermal decomposition of Zn/Al-LDH occurred in three steps (Fig. 6a). The first step was due to the evaporation of physisorbed water molecules on the exterior surface of Zn/Al-LDH, which occurred at 394.8 K with 5.5 % weight loss. The second decomposition that happened at 524.5 K with 15.3 % weight loss was due to the elimination of interlayer water molecules. The final step of Zn/Al-LDH decomposition was caused by the dihydroxylation of Zn/Al-LDH at 604.0 K with 8.58 % weight loss [43]. The thermal decomposition of pure CP occurred in one major weight loss step (Fig. 6b). Abrupt weight loss was observed at 453.1 K, with 99.1 % weight loss triggered by the decarboxylation reaction of CP, which produces two volatile products, namely CO<sub>2</sub> and 2,5-dichloropyridine [44].

The TGA curve of the Zn/Al-LDH-CP nanocomposite shows that the decomposition of the nanocomposite occurred in four steps. The first step was around 363.2 K (8.1 %) due to interlayer water elimination. The second step of thermal events occurred at 545.0 K with 13.9 % weight loss, attributed to the elimination of interlayer water. In the third step, the thermal decomposition occurred at 601.8 K, with the weight loss of 4.1 % due to the dihydroxylation of Zn/Al-LDH structure. It is noticeable from the TGA curve of Zn/Al-LDH-CP that no thermal decomposition occurred at 453.1 K, attributed to the decomposition of CP. Instead, a new broad peak appeared on the TGA curve of Zn/Al-LDH-CP at 117.4 K, which was observed neither for pure CP nor for the Zn/Al-LDH samples. It can be proposed that the decomposition of intercalated CP occurs *via* different mechanism than for pure CP. It is possible that the presence of Zn/Al-LDH acts as a catalyst that led to the polymerisation of the CP molecules intercalated in the interlayer gallery of Zn/Al-LDH. Hence, instead of decomposition *via* simple decarboxylation reaction as in pure CP (at 453.1 K), heating of Zn/Al-LDH-CP results in the formation of tarry and char substances; their oxidation and decomposition occur at significantly higher temperature (at 1117.4 K). The estimated weight loss of 23 % that occurs for Zn/Al-LDH-CP in the range of 1073–1173 K, is close enough to the content of CP (25.4 %) in the Zn/Al-LDH-CP sample (determined by an elemental analysis in subsequent section). Such similarity in these values can be considered as a good proof of the above scenario. Based on the results obtained from the thermal studies, it can be seen that the Zn/Al-LDH-CP nanocomposite had better thermal stability than Zn/Al-LDH and CP.

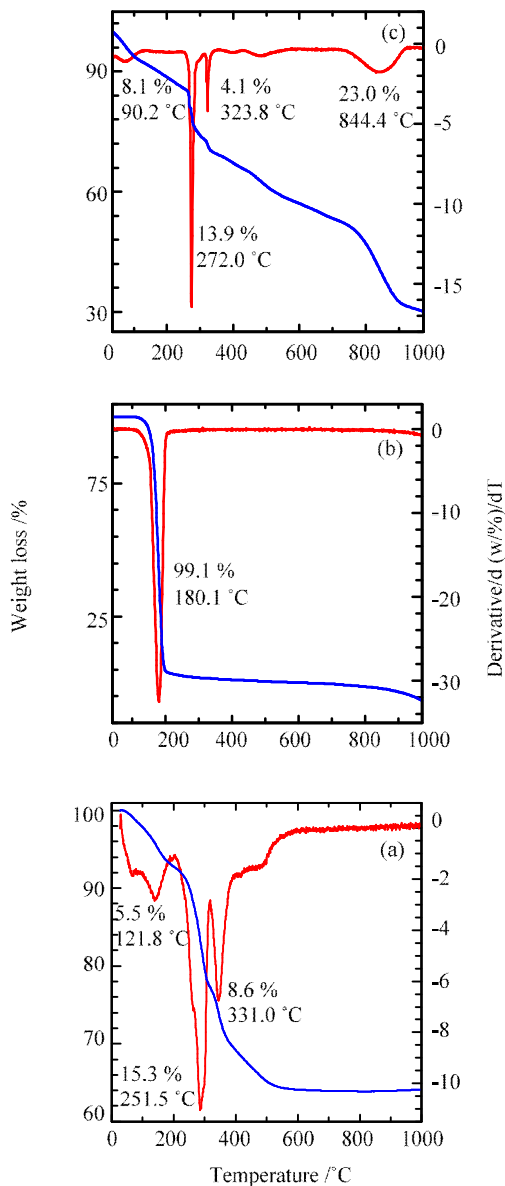


**Fig. 6.** TGA/DTG curves of Zn/Al-LDH (a), CP (b) and Zn/Al-LDH-CP (c) nanocomposites

### 3.5. Elemental Analysis

The chemical composition of Zn/Al-LDH, CP and Zn/Al-LDH-CP nanocomposites is represented in Table 1. Although the molar ratio of Zn/Al in the mother liquor of Zn/Al-LDH was 3.0, the elemental analysis conducted using ICP revealed that a final molar of Zn/Al in Zn/Al-LDH was slightly reduced to 2.9. The reduction is believed to occur because of the incomplete precipitation of Al<sup>3+</sup> during the formation of the positively charged layer in Zn/Al-LDH [48]. Based on the percentage of carbon in Zn/Al-LDH-CP (9.58 %), the amount of CP loaded in the nanocomposite was determined to be 25.39 %. The Zn/Al

molar ratio in Zn/Al-LDH-CP was consistent with the molar ratio of Zn/Al in the mother liquor, *i.e.* 3.0. On the basis of the results obtained from the TGA and

elemental analysis, the Zn/Al-LDH-CP nanocomposite can be formulated as  $[\text{Zn}_{0.75}\text{Al}_{0.25}(\text{OH})_2][\text{C}_5\text{H}_2\text{Cl}_2\text{NCOO}]_{0.25}\cdot 0.67\text{H}_2\text{O}$ .

Table 1

Elemental chemical composition of Zn/Al-LDH, CP and Zn/Al-LDH-CP nanocomposite

Sample	Zn/Al molar ratio ( $R_f$ )	C, %	H, %	N, %	Mole fraction		<sup>a</sup> CP, % w/w	<sup>b</sup> Formula
					$X_{\text{Zn}}$	$X_{\text{Al}}$		
Zn/Al-LDH	2.9	-	3.80	2.40	0.74	0.26	-	$[\text{Zn}_{0.74}\text{Al}_{0.26}(\text{OH})_2](\text{NO}_3)_{0.26}\cdot 0.22\text{H}_2\text{O}$
CP	-	37.37	1.54	7.17	-	-	-	$\text{C}_6\text{H}_3\text{Cl}_2\text{NO}_2$
Zn/Al-LDH-CP	3.0	9.58	2.60	2.46	0.75	0.25	25.39	$[\text{Zn}_{0.75}\text{Al}_{0.25}(\text{OH})_2][\text{C}_5\text{H}_2\text{Cl}_2\text{NCOO}]_{0.25}\cdot 0.67\text{H}_2\text{O}$

Notes: <sup>a</sup> estimated from CHNS analysis; <sup>b</sup> estimated from ICP-OES, CHNS and TGA/DTG analyses

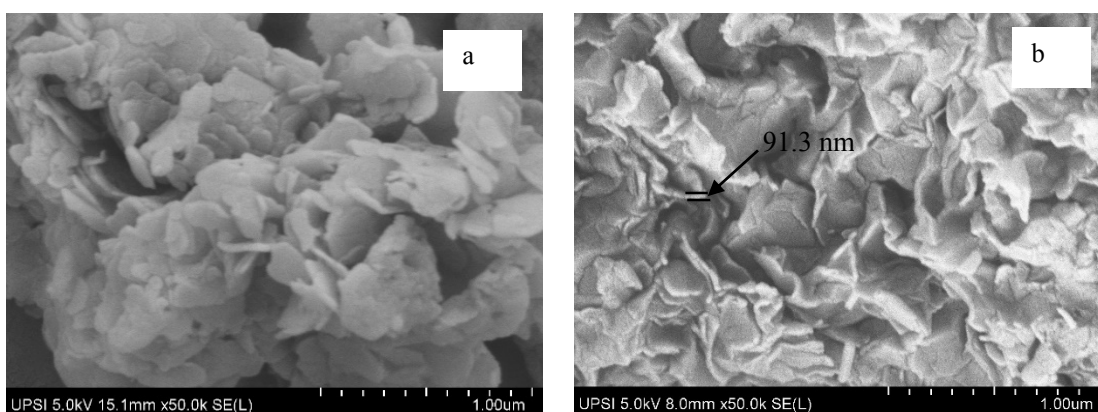


Fig. 7. Surface morphology of Zn/Al-LDH (a) and Zn/Al-LDH-CP (b) nanocomposites

### 3.6. Surface Morphology Analysis

The FESEM images of both pristine Zn/Al-LDH and the Zn/Al-LDH-CP nanocomposite are shown in Figs. 7a and 7b, respectively. The surface morphology analysis conducted on the samples reveals that Zn/Al-LDH appears as agglomerates, *i.e.* non-uniform, irregular and plate-like structures, which were expected to be based on the typical morphology of Zn/Al-LDH [36]. The Zn/Al-LDH-CP nanocomposites showed a similar morphology to pristine Zn/Al-LDH, but with a more compact arrangement. Based on the fact that both pristine Zn/Al-LDH and Zn/Al-LDH-CP showed a flake-like, thin lamellar sheet structure, it was quite obvious from these images that these materials possess a layered morphology [49].

### 3.7. Surface Property Analysis

The  $\text{N}_2$  adsorption-desorption isotherms of Zn/Al-LDH and the Zn/Al-LDH-CP nanocomposite are shown in Fig. 8. The adsorption-desorption of Zn/Al-

LDH showed a characteristic Type II isotherm which indicates a multilayer adsorption on a macroporous solid, whereas the Zn/Al-LDH-CP nanocomposite demonstrated a Type IV isotherm, characteristic of mesoporous materials (based on the classification provided by IUPAC). The  $\text{N}_2$  adsorption on Zn/Al-LDH and Zn/Al-LDH-CP took place slowly at low relative pressure, and increased rapidly at a higher relative pressure ( $P > 0.4$  for Zn/Al-LDH and  $P > 0.5$  for Zn/Al-LDH-CP). Optimum adsorption was achieved at 32 and 15.5  $\text{cm}^3\cdot\text{g}^{-1}$  for Zn/Al-LDH and Zn/Al-LDH-CP, respectively. The isotherm curve shows that H3 hysteresis was present in both curves; therefore, the particles were expected to have plate-like shape with slit-shaped pores [50]. The wider desorption branch of the hysteresis loop seen with Zn/Al-LDH in comparison with the hysteresis loop observed for Zn/Al-LDH-CP reveals different pore texture properties in these materials [38].

Regarding the BJH pore diameter distribution of the two samples, significant differences were observed

due to the fact that these samples showed dissimilar isotherms. The curves of BJH pore diameter desorption are illustrated in Fig. 9. The average pore diameter of Zn/Al-LDH was determined as 52.47 nm; however, after intercalation, the average pore diameter in Zn/Al-LDH-CP was reduced to 24.57 nm. In Zn/Al-LDH, three maxima peaks were observed at 2.4, 1.9 and 2.2 nm, whereas in Zn/Al-LDH-CP the maxima peaks emerged at 2.2, 4.2 and 6.3 nm. The total pore volume

of Zn/Al-LDH and Zn/Al-LDH-CP was found to be 0.012 and 0.080  $\text{cm}^3\cdot\text{g}^{-1}$ , respectively. The BET surface area was determined to be 0.901  $\text{m}^2\cdot\text{g}^{-1}$  for Zn/Al-LDH and 1.310  $\text{m}^2\cdot\text{g}^{-1}$  for Zn/Al-LDH-CP. The results on the surface properties of Zn/Al-LDH and the Zn/Al-LDH-CP nanocomposite are summarised in Table 2. Based on this analysis, it can be seen that the intercalation of CP into the interlayer gallery of Zn/Al-LDH led to changes in the surface properties.

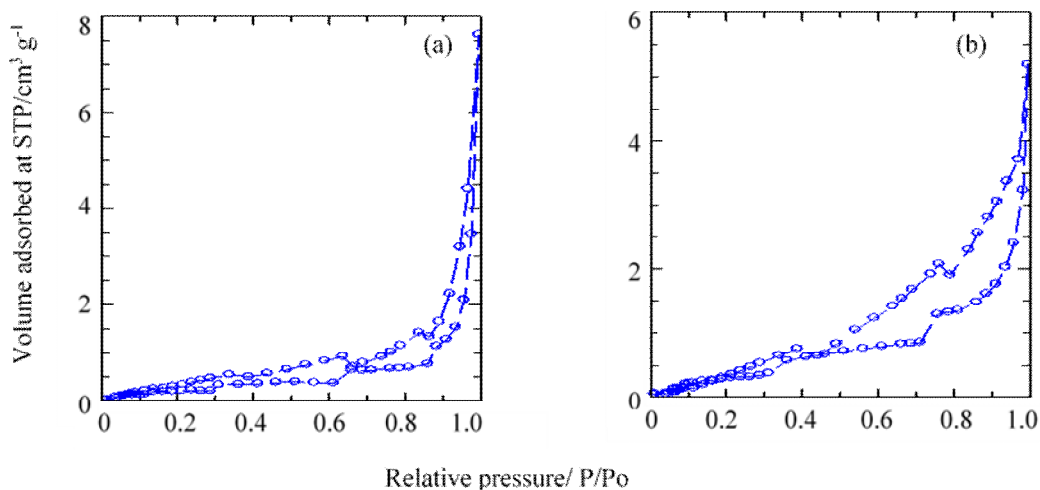


**Fig. 8.** Adsorption-desorption isotherms of nitrogen gas for Zn/Al-LDH (a) and Zn/Al-LDH-CP (b) nanocomposites

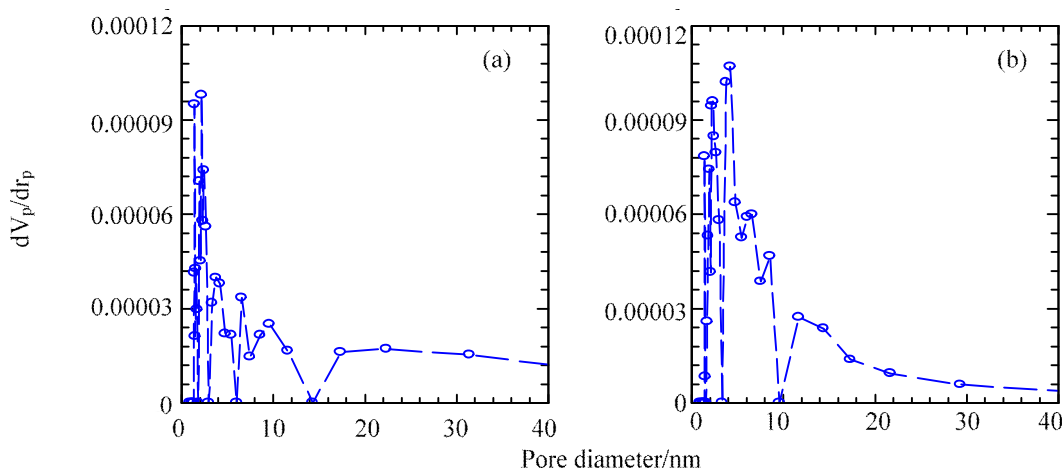


**Fig. 9.** BJH desorption pore size distributions for Zn/Al-LDH (a) and Zn/Al-LDH-CP (b) nanocomposites

Table 2

**Surface properties of Zn/Al-LDH and Zn/Al-LDH-CP nanocomposites**

Sample	Basal spacing, Å	Total pore volume, $\text{cm}^3\cdot\text{g}^{-1}$	Multipoint BET surface area, $\text{m}^2\cdot\text{g}^{-1}$	BJH average pore diameter, nm
Zn/Al-LDH	8.90	0.012	0.901	52.470
Zn/Al-LDH-CP	15.7	0.080	1.310	24.57

## 4. Conclusions

The fabricated material Zn/Al-LDH was successfully intercalated with an auxin mimic herbicide (CP) using the co-precipitation method. The PXRD data reveal that there was a significant increase in the height of the interlayer gallery, and based on the value of the basal spacing, it can be proposed that CP was oriented in a monolayer arrangement. The success of intercalation was also supported by the results from the FTIR and elemental analysis. The thermal stability studies showed that the Zn/Al-LDH-CP nanocomposite possess better thermal stabilities than the pure CP. The intercalation of CP into the interlayer gallery of Zn/Al-LDH also led to some changes in the surface morphology and surface properties. All these characterisation results show the very promising future of this novel Zn/Al-LDH-CP nanocomposite, and suggest that this nanocomposite will certainly find applications in agriculture.

## Acknowledgements

The author wish to thank University Pendidikan Sultan Idris and Ministry of Education of Malaysia for the support during this research. This work was supported by the University Pendidikan Sultan Idris under GPU Grant No. 2017-0188-101-01 and Ministry of Education of Malaysia under FRGS Grant No. 2017-0075-101-02.

## References

- [1] Schubert U., Hüsing N.: *Synthesis of Inorganic Materials*, 3<sup>rd</sup> edn. John Wiley & Sons. Weinheim 2012.
- [2] Saber O., Tagaya H.: *J. Porous Mater.*, 2009, **16**, 81. <https://doi.org/10.1007/s10934-007-9171-x>
- [3] Kuzma J.: *Livest. Sci.*, 2010, **130**, 14. <https://doi.org/10.1016/j.livsci.2010.02.006>
- [4] Martín-Yerga D., González-García M., Costa-García A.: *Sensor. Actuat. B*, 2012, **165**, 143. <https://doi.org/10.1016/j.snb.2012.02.031>
- [5] Ghotbi M., Hussein M., Yahaya A., Rahman M.: *J. Phys. Chem. Solids*, 2009, **70**, 948. <https://doi.org/10.1016/j.jpcs.2009.05.007>
- [6] Cursino A., Gardolinski J., Wypych F.: *J. Colloid Interf. Sci.*, 2010, **347**, 49. <https://doi.org/10.1016/j.jcis.2010.03.007>
- [7] Chiu C., Huang T., Wang Y. *et al.*: *Progr. Polym. Sci.*, 2014, **39**, 443. <https://doi.org/10.1016/j.progpolymsci.2013.07.002>
- [8] Hong J., Zhu Z., Lu H., Qiu Y.: *Chem. Eng. J.*, 2014, **252**, 267. <https://doi.org/10.1016/j.cej.2014.05.019>
- [9] Jaeger S., Zimmermann A., Zawadzki S. *et al.*: *Polimeros*, 2014, **24**, 683. <https://doi.org/10.1590/0104-1428.1733>
- [10] Choy J., Son Y.: *Bull. Korean Chem. Soc.*, 2004, **25**, 122. <https://doi.org/10.5012/bkcs.2004.25.1.122>
- [11] Berber M., Hafez I., Minagawa K.: [in:] Hashim A. (Ed.), *Advance in Nanocomposite Technology*. InTech. Rijeka 2011. 335-360. <https://doi.org/10.5772/676>
- [12] Schneiderová B., Pleštil J., Tarábková H. *et al.*: *Dalton T.*, 2014, **43**, 10484. <https://doi.org/10.1039/c4dt00141a>
- [13] Ragavan A., Khan A., O'Hare D.: *J. Phys. Chem. Solids*, 2006, **67**, 983. <https://doi.org/10.1016/j.jpcs.2006.01.076>
- [14] Valente J., Tzompantzi F., Prince J. *et al.*: *Appl. Catal. B*, 2009, **90**, 330. <https://doi.org/10.1016/j.apcatb.2009.03.019>
- [15] Zhenlan Q., Heng Y., Bin Z., Wanguo H.: *Colloid Surface A*, 2009, **348**, 164. <https://doi.org/10.1016/j.colsurfa.2009.07.004>
- [16] Lu P.: *Polym. Plast. Technol. Eng.*, 2010, **49**, 1450. <https://doi.org/10.1080/03602559.2010.496415>
- [17] Nejati K., Davary S., Saati M.: *Appl. Surf. Sci.*, 2013, **280**, 67. <https://doi.org/10.1016/j.apsusc.2013.04.086>
- [18] Chaara D., Pavlovic I., Bruna F. *et al.*: *Appl. Clay Sci.*, 2010, **50**, 292. <https://doi.org/10.1016/j.clay.2010.08.002>
- [19] He J., Wei M., Li B. *et al.*: *Preparation of Layered Double Hydroxides*. [in:] Duan *et al.* (Eds.), *Layered Double Hydroxides*. Springer-Verlag Berlin Heidelberg 2006, 89–119. [https://doi.org/10.1007/430\\_006](https://doi.org/10.1007/430_006)
- [20] Touloupakis E., Margelou A., Ghanotakis D.: *Pest. Manag. Sci.*, 2011, **67**, 837. <https://doi.org/10.1002/ps.2121>
- [21] Qiu D., Hou W., Xu J. *et al.*: *Chinese J. Chem.*, 2009, **27**, 1879. <https://doi.org/10.1002/cjoc.200990315>
- [22] Park M., Lee C., Seo Y. *et al.*: *Environ. Sci. Pollut. Res.*, 2010, **17**, 203. <https://doi.org/10.1007/s11356-009-0235-0>
- [23] Grover K., Komarneni S., Katsuki H.: *Appl. Clay Sci.*, 2010, **48**, 631. <https://doi.org/10.1016/j.clay.2010.03.017>
- [24] Jin S., Fallgren P., Morris J., Chen Q.: *Sci. Technol. Adv. Mater.*, 2007, **8**, 67. <https://doi.org/10.1016/j.stam.2006.09.003>
- [25] Carja G., Kameshima Y., Nakajima A. *et al.*: *Int. J. Antimicrob. Agents*, 2009, **34**, 534. <https://doi.org/10.1016/j.ijantimicag.2009.08.008>
- [26] Mishra G., Dash B., Pandey S., Mohanty P.: *J. Environ. Chem. Eng.*, 2013, **1**, 1124. <https://doi.org/10.1016/j.jece.2013.08.031>
- [27] Ryu S., Jung H., Oh J. *et al.*: *J. Phys. Chem. Solids*, 2010, **71**, 685. <https://doi.org/10.1016/j.jpcs.2009.12.066>
- [28] Isa I., Sharif S., Hashim N., Ghani S.: *Ionics (Kiel)*, 2015, **3**, 1.
- [29] Mokhtar M., Saleh T., Ahmed N. *et al.*: *Ultrason. Sonochem.*, 2011, **18**, 172. <https://doi.org/10.1016/j.ultsonch.2010.05.001>
- [30] Bovey R.: *Woody Plants and Woody Plant Management*. Marcel Dekker Inc. New York 2001.
- [31] Roberts T. (Ed.): *Metabolic Pathways of Agrochemicals*. The Royal Society of Chemistry. Cambridge 1998.
- [32] Tu M., Hurd C., Randall J.: *Weed Control Methods Handbook*. The Nature Conservancy 2003.
- [33] Hussein M., Hashim N., Yahaya A., Zainal Z.: *Sains Malaysiana*, 2011, **40**, 887.
- [34] Bashi A., Hussein M., Zainal Z. *et al.*: *Arab. J. Chem.*, 2016, **9**, 1457. <https://doi.org/10.1016/j.arabjc.2012.03.015>
- [35] Barahuie F., Hussein M., Arulselvan P. *et al.*: *J. Solid State Chem.*, 2014, **217**, 31. <https://doi.org/10.1016/j.jssc.2014.04.015>
- [36] Sarijo S., Ghazali S., Hussein M., Sidek N.: *J. Nanopart. Res.*, 2013, **15**, 1. <https://doi.org/10.1007/s11051-012-1356-9>
- [37] Mac Hado G., Arizaga G., Wypych F., Nakagaki S.: *J. Catal.*, 2010, **274**, 130. <https://doi.org/10.1016/j.jcat.2010.06.012>
- [38] Sarijo S., Ghazali S., Hussein M., Ahmad A.: *Mater. Today Proc.*, 2015, **2**, 345. <https://doi.org/10.1016/j.matpr.2015.04.061>
- [39] Liu P., Wang H., Feng Z. *et al.*: *J. Catal.*, 2008, **256**, 345. <https://doi.org/10.1016/j.jcat.2008.03.022>
- [40] Davila V., Lima E., Bulbulian S., Bosch P.: *Micropor. Mesopor. Mater.*, 2008, **107**, 240. <https://doi.org/10.1016/j.micromeso.2007.03.013>

- [41] Hussein M., Jubri Z., Zainal Z., Yahya A.: Mater. Sci.-Poland, 2004, **22**, 57
- [42] Li S., Shen Y., Xiao M. et al.: Arab. J. Chem., 2015. <https://doi.org/10.1016/j.arabjc.2015.04.034>
- [43] Fernandez J., Ulibarri M., Labajos F., Rives V.: J. Mater. Chem., 1998, **8**, 2507.
- [44] Clark L.: J. Phys. Chem., 1962, **66**, 125. <https://doi.org/10.1021/j100807a026>
- [45] Qiu L., Chen W., Qu B.: Polym. Degrad. Stab., 2005, **87**, 433. <https://doi.org/10.1016/j.polymdegradstab.2004.09.009>
- [46] Prasanna S., Kamath P.: J. Colloid Interf. Sci., 2009, **331**, 439. <https://doi.org/10.1016/j.jcis.2008.11.054>
- [47] Gasser M., Aly H.: Colloid Surface A, 2009, **336**, 167. <https://doi.org/10.1016/j.colsurfa.2008.11.047>
- [48] Whilton N., Vickers P., Mann S.: J. Mater. Chem., 1997, **7**, 1623. <https://doi.org/10.1039/a701237c>
- [49] Arizaga G., Satyanarayana K., Wypych F.: Solid State Ionics, 2007, **178**, 1143. <https://doi.org/10.1016/j.ssi.2007.04.016>
- [50] Geng C., Xu T., Li Y. et al.: Chem. Eng. J., 2013, **232**, 510. <https://doi.org/10.1016/j.cej.2013.08.010>

Received: May 16, 2018 / Revised: September 21, 2018 /  
Accepted: October 25, 2018

## ІНТЕРКАЛЯЦІЙНА ПОВЕДІНКА І ФІЗИКО-ХІМІЧНА ХАРАКТЕРИСТИКА НОВОГО ІНТЕРКАЛЬОВАНОГО НАНОКОМПЗИТУ З ПОДВІЙНОГО ГІДРОКСИДУ ЦИНКУ/АЛЮМІНІЮ ТА КЛОПІРАЛІДУ З ШИРОКОЛИСТЯНИХ ГЕРБІЦИДІВ

**Анотація.** *Методом спільного осадження одержані нові наноккомпозити, що містять подвійний гідроксид цинку/алюмінію інтеркальований клопіралідом (Zn/Al-LDH-CP). За допомогою порошкової дифракції (PXRD) підтверджено виникнення інтеркаляції. Встановлено, що результати Фур'є спектроскопії та елементного аналізу узгоджуються з результатами PXRD, та підтверджують інтеркаляцію клопіраліду. За допомогою термічних методів аналізу показано, що термічну стійкість наноккомпозиту є вищою у порівнянні з чистим клопіралідом. Запропонована хімічна формула наноккомпозиту  $[Zn_{0.75}Al_{0.25}(OH)_2][C_5H_2Cl_2NCOO] \cdot 0.250.67H_2O$  та розраховано вміст клопіраліду в Zn/Al-LDH (25,39%). Приведені перспективи використання нового наноккомпозиту Zn/Al-LDH-CP.*

**Ключові слова:** *подвійний гідроксид цинку/алюмінію, спільне осадження, клопіралід, інтеркаляція, гербіцид.*